VOL. 16, NO. 14, JULY 2021 ISSN 1819-6608
ARPN Journal of Engineering and Applied Sciences

www.arpnjournals.com

EFFECTS OF ENTRY CONDITIONS ON CHANNEL FLOW CHARACTERICSTICS

Oyewola O. M.[1], Singh P.M.[1], Odele R. P.[2] and Petinrin M. O.[2]
[1]School of Mechanical Engineering, Fiji National University, Suva, Fiji
[2]Department of Mechanical Engineering, University of Ibadan, Ibadan, Nigeria
E-Mail: oooyewola001@gmail.com

ABSTRACT

There have been various studies on channel flow due to its relevance in engineering applications, but the effects of the entry conditions on its flow characteristics have not been given much attention. This 2-D numerical simulation studied how the initial velocity and tripping devices at the entrance of a channel affect the mean flow structure. The CFD analysis is based on the use of COMSOL Multiphysics. The turbulent stresses in the RANS equation are closed using the *k-ε* turbulence model. Input parameters for the simulation are taken from experimental conditions in the literature, with Reynolds number ranging from 18,700 to 600, 000. The CFD strategy flow without tripping is validated against experimental results and a good agreement is achieved. The results show that the skin friction factor for the flow without tripping for Reynolds number 18,700 is $3.59x10^{-3}$. However, for the same Re, with tripping devices covering 15%, 30%, 45%, and 60% of the channel height, the skin friction factors are $3.68x10^{-3}$, $3.78x10^{-3}$, $3.82x10^{-3}$, and $3.98x10^{-3}$ respectively. Hence it has been shown the tripping devices placed at the entry of a channel increase the skin friction coefficient by values between 2% to 11% for the various conditions considered in this work.

Keywords: entry conditions, channel flow, skin friction, Reynolds number, tripping devices.

1. INTRODUCTION

Channel flow can be described as a three-dimensional flow which is widely affected by the effects of free surface currents and the side walls. The velocity profiles of open channel flow are of great interest to engineers as it has practical consequences in the estimation of erosion effects and transportation of sediments in alluvial channels. Over the years much work has been done on studying channel flow. Tominaga *et al.* (1989) noted, from their experimental studies on the three-dimensional turbulent structure of channel flow, that the secondary currents observed in open channel flows are quite different from those in closed channel flows. Cardoso *et al*. (1989) in their experiments on uniform flow in smooth open channel noted that a wide two-dimensional region existed in the center, which was free of effects of secondary currents. This observation is in agreement with the results of Kirkgoz (1989), Tominaga *et al*. (1992), Kirkgoz and Ardichoglu (1997), and Nezu (2005). All these authors thus corroborate that for an aspect ratio (width to depth ratio of the flow, B/H) $B/H \geq 5$, there exists a predominant two-dimensional region for which the effects of secondary currents aren't felt. Thus for channels with a smaller aspect ratio ($B/H<5$), the effects of free surface currents and the side walls are predominant on the flow, and the maximum velocity on the channel centerline is observed to be below the surface - dip phenomenom (Yang *et al*., 2004, Yan *et al*., 2011, Al Faruque *et al*., 2014, Bonakdari *et al*., 2014). Hence, studies in open channel flow have also revealed that the classical log law gives a good description of the velocity distribution in the inner region (Yan *et al*., 2004, Nezu, 2005, Alfaz *et al*., 2009, Al Faruque *et al*., 2014) and the extent of collapse of the mean velocity profile - in inner scaling - with the log region is dependent on the Reynolds number (Alfaz *et al*., 2009, Al Faruque *et al*., 2004).

In the entrance and very close to the channel bed in open channel flows, the velocity gradients are always high as the boundary layer grows, laminar flow is hardly encountered in practice and so much more attention is being paid to turbulent flow (Bonakdari *et al*., 2014). However, there is a transition from laminar to turbulent boundary layer near the leading edge (Figure-1).

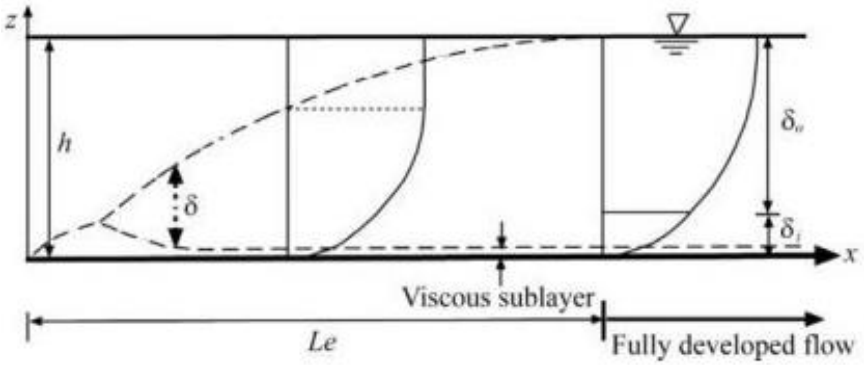

Figure-1. Velocity profiles in developing and fully developed open channel flow (Bonakdari *et al*., 2014; Kirkgoz and Ardichoglu, 1997).

Tripping devices are known to cause immediate transition from a laminar to a turbulent boundary layer, and cause a more fully developed flow sooner. A tripping device could be a ring, a cylinder, sandpaper, or some rough element. Most channel flow experiments make use of tripping devices to cause immediate transition, however much attention has not been paid to how tripping affects the characteristics of a flow. Al-Salaymeh and Bayoumi (2009) did an experimental investigation of tripping effect on the friction factor in turbulent pipe flows by installing tripping devices for different blocking areas: 10%, 20%, 30% and 40%, at the pipe entrance. Their results suggested that there is an insignificant effect on the friction factor as the blocking area (dimension of trip device) increased, but the centerline velocity decreased with an increase in the blocking area.

In this present work, the effects of initial velocity and tripping devices with blocking areas: 15%, 30%, 45%, and 60%, of flow parameters in an open channel flow will be solved numerically.

2. METHODOLOGY

The present numerical study makes use of COMSOL Multiphysics commercial CFD package. The software is a finite-element method solver, and solves for the velocity field across all sections.

2.1 Governing Fluid Flow Equations

The two governing equations adopted for modeling the steady and incompressible flow in open channel are:

a) The law of conservation of mass

$$\frac{\partial U_j}{\partial x_j} = 0 \tag{1}$$

b) The Reynolds time averaged Navier-Stokes (RANS) equation.

$$\frac{\partial U_i}{\partial t} + U_j \frac{\partial U_i}{\partial x_j} = -\frac{1}{\rho}\frac{\partial P}{\partial x_i} + \frac{\partial}{\partial x_j}\left[\upsilon\left(\frac{\partial U_i}{\partial x_j} + \frac{\partial U_j}{\partial x_i}\right) - \overline{u_i' u_j'}\right] \tag{2}$$

where x_i represents the coordinate axis, U_i's represent the stream velocities in the streamwise and vertical direction, z is the vertical elevation and ρ represents the density, P represents the pressure, and $\overline{u_i' u_j'}$ is the specific Reynolds stress tensor.

2.2 Turbulence Closure

Applying the Boussinesq approximation to obtain the eddy viscosity model, the specific Reynolds stress tensor in equation (2) is given as (Ferziger and Peric, 2002; Wilcox, 2006)

$$-\overline{u_i' u_j'} = \upsilon_T\left(\frac{\partial U_i}{\partial x_j} + \frac{\partial U_j}{\partial x_i}\right) - \frac{2}{3}k\delta_{ij}$$

Thus, the k-ε turbulence equations are employed to obtain the closed form solution of the eddy viscosity model and the equations are as given

$$U_j \frac{\partial k}{\partial x_j} = \frac{\partial}{\partial x_j}\left[\left(\upsilon + \frac{\upsilon_T}{\sigma_k}\right)\frac{\partial k}{\partial x_j}\right] + \left[\upsilon_T\left(\frac{\partial U_i}{\partial x_j} + \frac{\partial U_j}{\partial x_i}\right) - \frac{2}{3}k\delta_{ij}\right]\frac{\partial U_i}{\partial x_j} - \varepsilon$$

$$U_j \frac{\partial \varepsilon}{\partial x_j} = \frac{\partial}{\partial x_j}\left[\left(\upsilon + \frac{\upsilon_T}{\sigma_\varepsilon}\right)\frac{\partial \varepsilon}{\partial x_j}\right] + C_{\varepsilon 1}\frac{\varepsilon}{k}\left[\upsilon_T\left(\frac{\partial U_i}{\partial x_j} + \frac{\partial U_j}{\partial x_i}\right) - \frac{2}{3}k\delta_{ij}\right]\frac{\partial U_i}{\partial x_j} - C_{\varepsilon 2}\frac{\varepsilon^2}{k}$$

where $\upsilon_T = C_\varphi \frac{k^2}{\varepsilon}$

The constants in the two-equation eddy-viscosity model have values given below
$C_{\varepsilon 1} = 1.44$, $C_{\varepsilon 2} = 1.92$, $C_\varphi = 0.09$, $\sigma_k = 1.0$, $\sigma_\varepsilon = 1.3$

2.3 Boundary Conditions

Boundary conditions are required in order to solve the governing equations around the computational domain.

a) The velocity inlet condition is set at the inlet of the domain
b) The pressure outlet condition is set at the exit of the domain i.e. gauge pressure = 0
c) The wall-function method is utilized at the bottom wall and the walls of the trip devices, which assumes a predictable behavior of the viscous sub-layer
d) The slip boundary condition is set at the free surface of the domain

2.4 Computational Grid

The computational domain is made up of a rectangular channel of length 9.5m, and height 0.1m (Figure-2). The computational domain is made up of a hybrid of structured and unstructured meshes. A structured boundary layer mesh is required at the base of the domain and around the trip cylinder. The domain contains very large cell densities around the entry and at the free surface of the flow, and higher cell density around the bottom wall and the trip cylinder. Relatively fine triangular and quadrilateral elements are used in the rest of the flow domain. Five different computational domains are set up to simulate the different trip conditions of the flow.

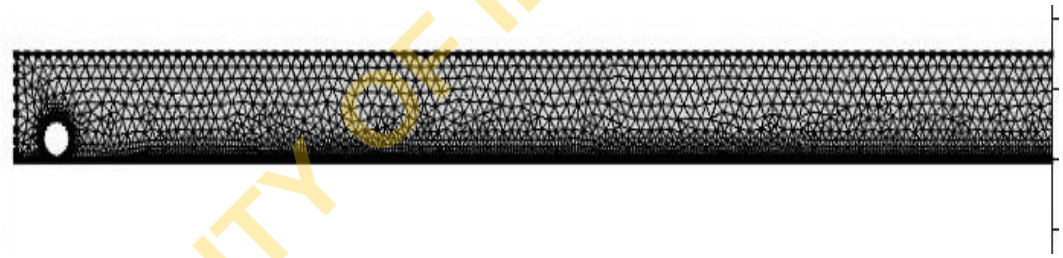

Figure-2. Two-dimensional computational domain in which the circle (trip cylinder) covers a certain percentage of the channel height.

2.5 Simulation Parameters

Data is taken from test conditions utilized in experiments of Tominaga *et al.* (1989). The experimental study was carried out in smooth and rough rectangular open channels. The results were obtained in a channel with 12.5 m length, and a square cross section (0.40 m × 0.40 m). The experiments were performed with the Reynolds number equal to 19,000 and Froude number equal to 0.19 for a depth of flow equal to 0.10 m and the mean velocity equal to 0.187 m/s. Velocity measurements were performed using a hot-film anemometer.

2.6 The Friction Velocity and Skin Friction Factor

Friction velocities are obtained at various positions in the streamwise direction of the flow in both the trip and the no trip cases. The velocity profiles are obtained at the various positions. These profiles are exported for post-processing. The friction velocity is obtained through the least-squares method, and comparing with prandtl-von-karman law of the wall equation

$$\frac{u}{u^*} = \frac{1}{\kappa}\ln y\frac{u^*}{\upsilon} + B$$

Where $K = 0.39$ (Von Karman constant) and $B = 5.5$, and u is the velocity along the profile, and a vertical distance y.

The skin-friction coefficient is calculated by

$$C_f = 2\left(\frac{u^*}{U_e}\right)^2$$

where U^* is the friction velocity and U_e is the free stream velocity. For comparison, the streamwise velocity profiles are then obtained for the no-trip flow, 15% trip, 30% trip, 45% trip, and 60% trip at the fully developed section x=6.5m

3. RESULTS AND DISCUSSIONS

3.1 Validation of Simulation Results

In Table-1, the simulation results for the flow without tripping are compared with data obtained in the experiments under various conditions, of Kirkgoz and Ardichoglu (1997). The simulation results compare well with the experimental data.

Table-1. Comparison of experimental and simulation data.

Test Number	h	Fr	Re	U* experimental (mm/s)	U* simulation (mm/s)
1	0.05	0.3	10500	9.7	8.7
2	0.025	0.85	10500	21.2	22.1
3	0.075	0.67	20025	23.5	22
4	0.1	0.34	33300	16.5	15.3
5	0.08	0.68	48320	30.8	27
6	0.15	0.36	64950	20.8	18.9
7	0.12	0.5	65040	25.7	23.5
8	0.1	0.66	65000	29.8	27.5

Hence in order to quantitatively compare the numerical model with the experimental results two indicators, relative error (R_{err}) and root-mean-square error ($RMSE$) were used:

$$R_{err} = \frac{1}{n}\sum_{i=1}^{n}\left|\frac{U_{mo} - U_{\exp}}{U_{\exp}}\right|$$

$$RMSE = \sqrt{\frac{1}{n}\sum_{i=1}^{n}\left(\frac{U_{mo} - U_{\exp}}{U_{\exp}}\right)^2}$$

where U_{mo} is the estimated friction velocity from the simulation, and U_{exp} is the estimated friction velocity from the experiments. Values of R_{err} = 7.2% and RMSE = 8.6% show there is reasonable agreement between the experimental and the simulation results. Also, it should be noted that the friction velocity in the experiments was obtained by point-wise measurements in the viscous sublayer; in the simulation results the friction velocity are obtained by estimating the logarithmic region of the wall.

3.2 Flow Development

The developed section of a flow is very important as that is where reasonable measurements of a flow's properties are taken. The flow is checked for full development by comparing the velocity profiles at various stream wise positions x = 1.1, 1.7, 2.5, 3.0, 3.5, 4.0, 4.5, 5.0, 5.5, 6.5, 7.0. Full development of the flow was assumed to be achieved when the velocity profiles witnessed no significant changes. From Figure-3, the variation in velocity profiles can be noticed at various stream wise positions in the developing region of the flow. In Figure-4, the absolute collapse in velocity profiles can be seen which indicates a fully developed flow. Thus for this flow condition i.e. v = 0.187m/s and h = 0.10m, the entry length is determined to be 6.5m or 65h. This observation is in agreement with literature where it is suggested that the development length is placed around 50h-70h.

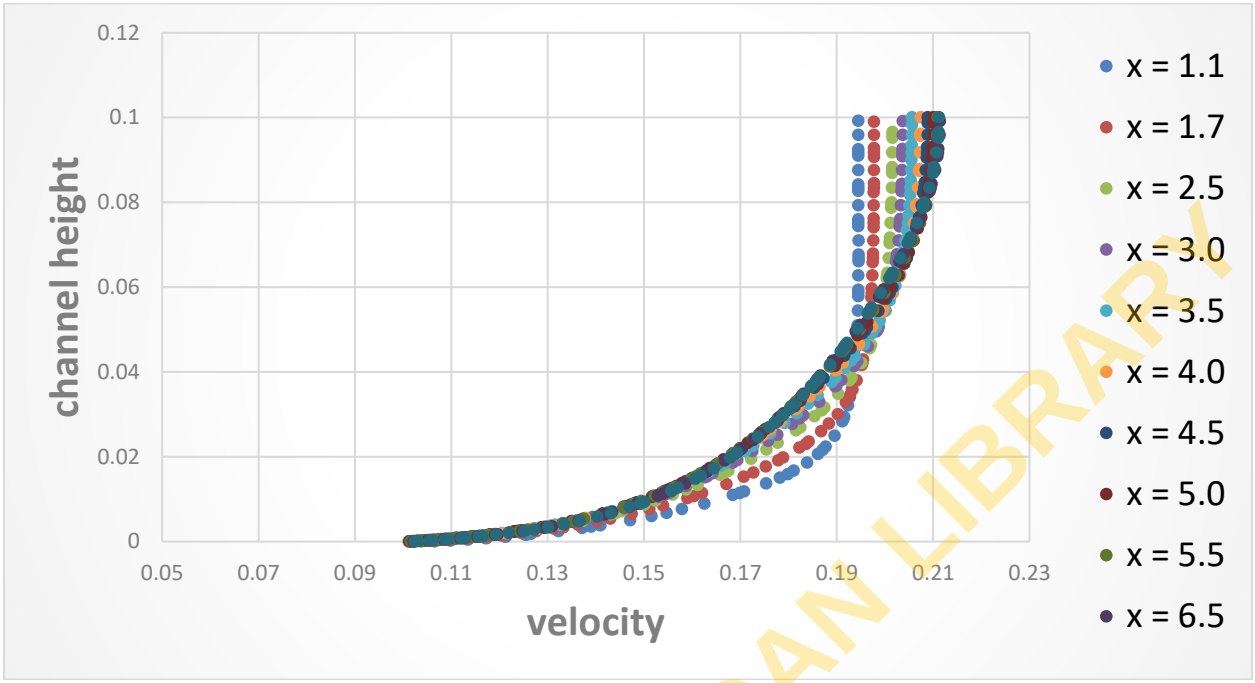

Figure-3. Velocity profiles at different streamwise positions in the channel.

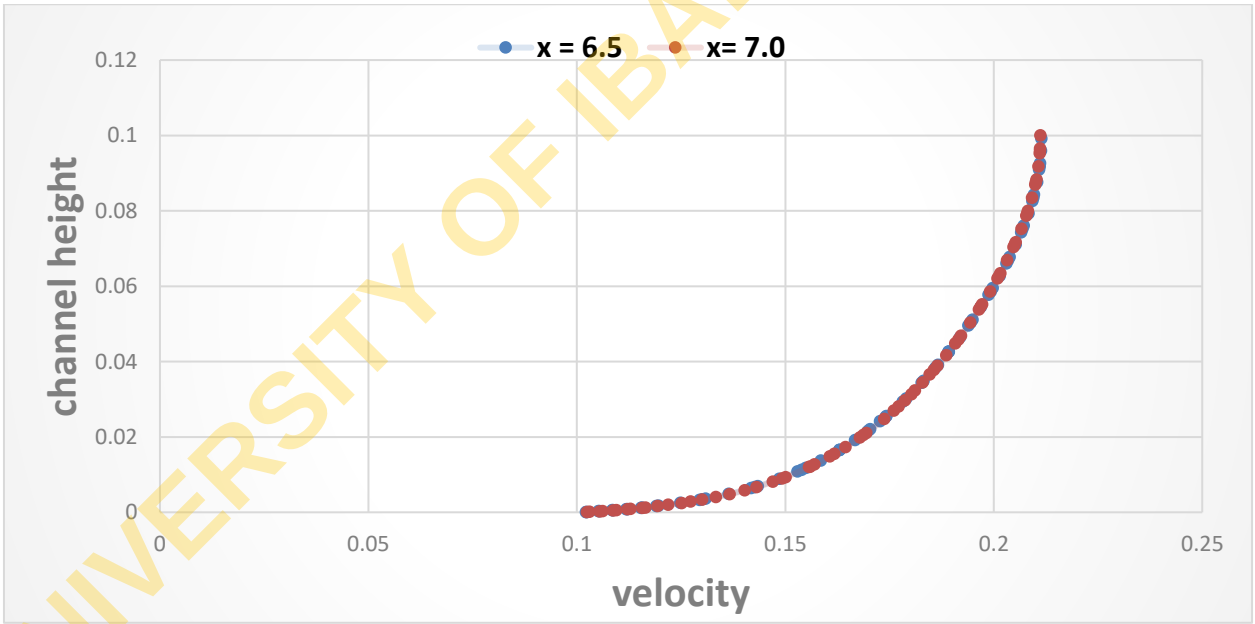

Figure-4. Velocity profiles at streamwise positions for x = 6.5m, and x=7.0m.

3.3 Variation of Friction Velocity Along Channel Length

The results of the simulation reveal that the friction velocity (and thus the bed shear stress) is maximum near the entrance (i.e. at x=0), and it decreases gradually in the developing region, becoming constant in towards the end of the developing region and further downstream (Table-2, Figure-5). This is in agreement with the work of Ranga Raju *et al*. (2000) who made similar observations in their experiments.

Table-2. Calculated shear velocities for flow without tripping.

Re	x = 1.1	x = 1.7	x = 2.5	x = 3.0	x = 4.0	x = 5.5	x = 6.5
18700	10	9.3	9.1	9	8.9	8.9	8.9
60000	28.5	26.9	26.2	26	25.9	25.5	25.5
131000	55.7	54.9	54	53.7	53.3	52.9	52.7
240000	96.3	94.9	93.9	93.7	93	92.2	91.9
330000	129	127	126	125	125	123	123
420000	163	160	158	158	155	154	153
600000	225	224	219	218	216	214	213

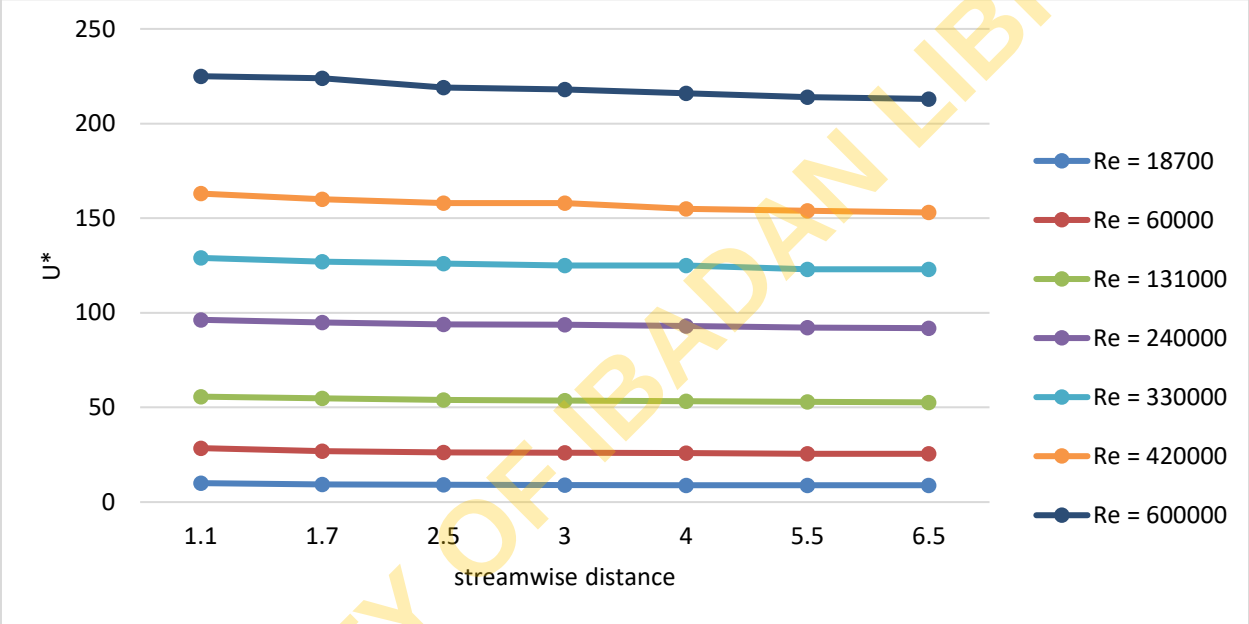

Figure-5. Plot of variation of shear velocity with streamwise location.

3.4 Reynolds Number and Skin Friction Relationship

The relationship mentioned in section 2.6 between skin friction coefficient and friction velocity, is used to obtain the relationship between the Reynolds number and skin friction coefficient for the various test conditions.

Figure-6 shows the relationship between friction factor and Reynolds number. The trend observed and results obtained are in good agreement with previous research works. From Figure-7, the effect of tripping on skin friction factor can be deduced. It can be seen that there is an increase in the value of the skin friction coefficient as the degree of tripping is increased. However, this increase is negligible. The observed trend is in agreement with observations made by Al-Salaymeh and Bayoumi (2009) in their experiments on the effects of entry conditions on friction factor in pipe flow. This is agreeable as pipe and channel flow have similar structures. It should as well thus be noted that the increase in skin friction factor for the flow conditions in this numerical experiment range between 2 and 11%.

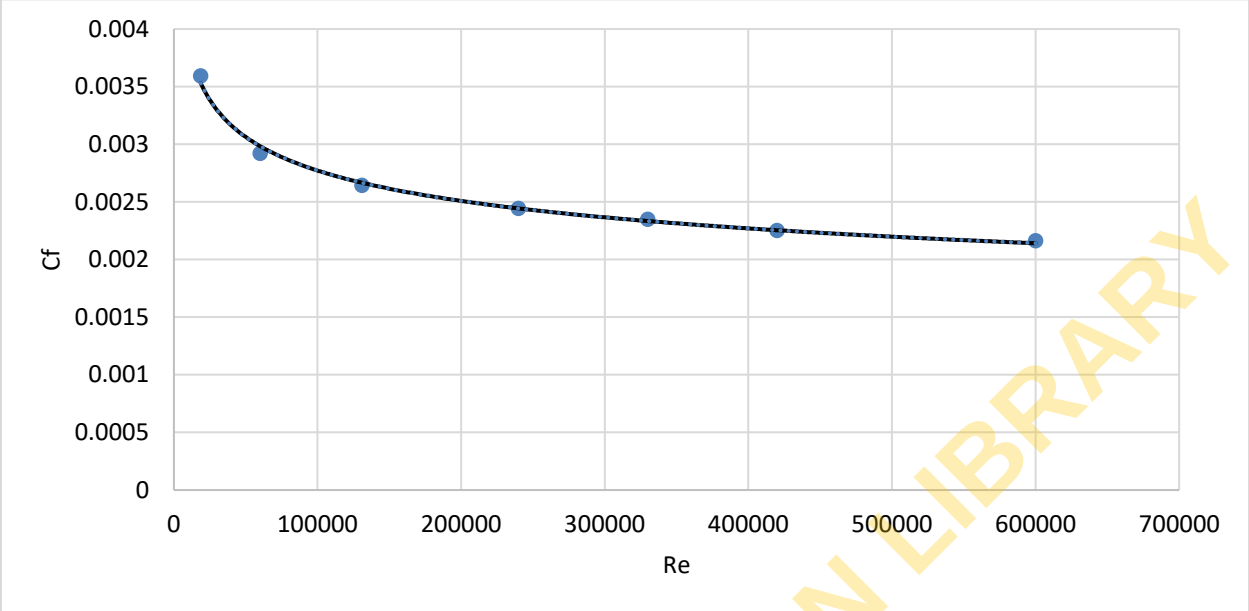

Figure-6. Friction factor vs Reynolds number.

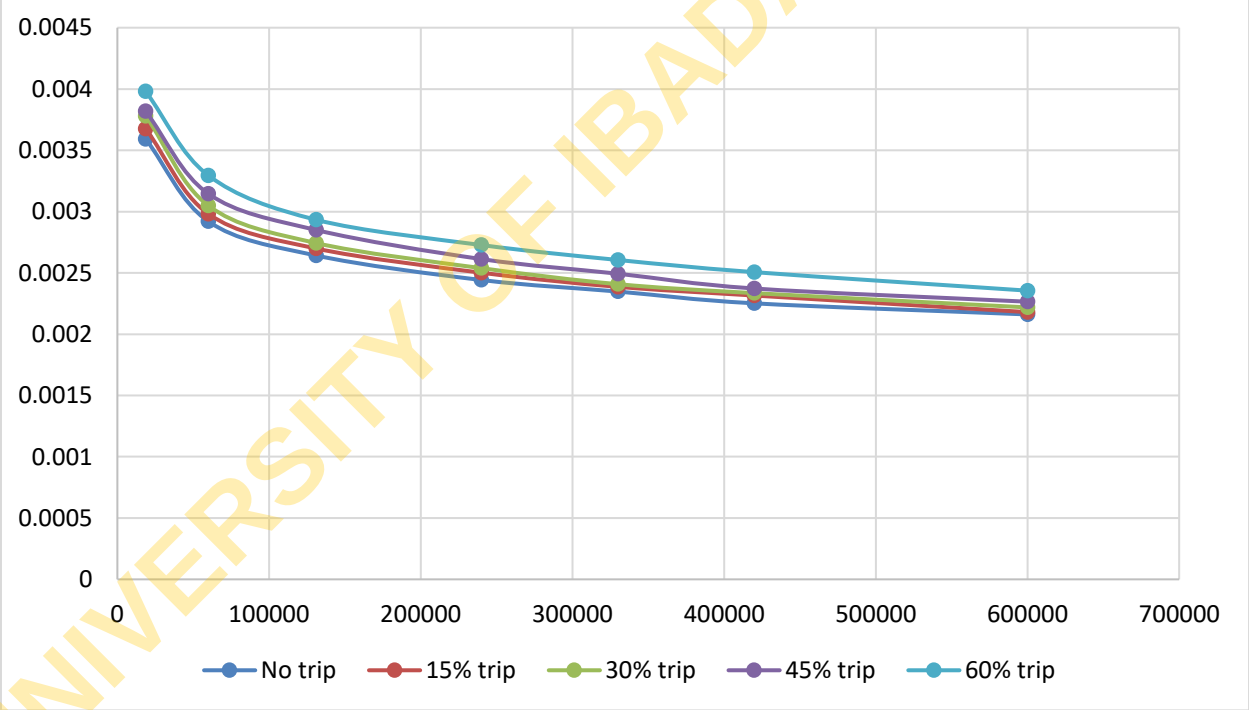

Figure-7. Friction factor and Reynolds number for various degrees of tripping.

3.5 Mean Velocity Profile: Inner Scaling

The distributions of the streamwise component of the mean velocity in inner scaling for various flow conditions are shown below. Friction velocity was calculated using least-squares method by fitting the logarithmic law of the wall expression with a best fit line drawn in the inner region of the velocity profile. As shown in Figure-8 and Figure-9, all data obtained in both the non-trip flow and the tripped flow show good agreement with the log law of the wall. It should be noted however that the standard k-ϵ turbulence model with wall-functions which is utilized does not resolve the viscous sub-layer and is thus not represented in the chart.

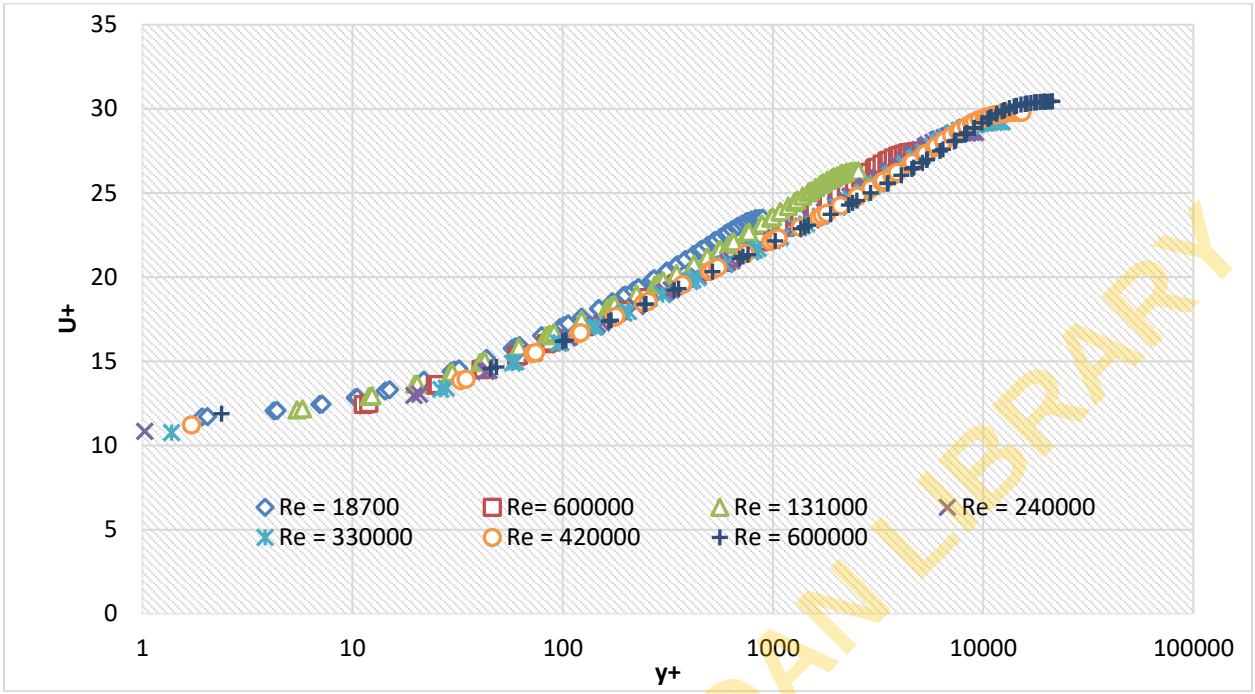

Figure-8. Normalized velocity distribution for flow without tripping.

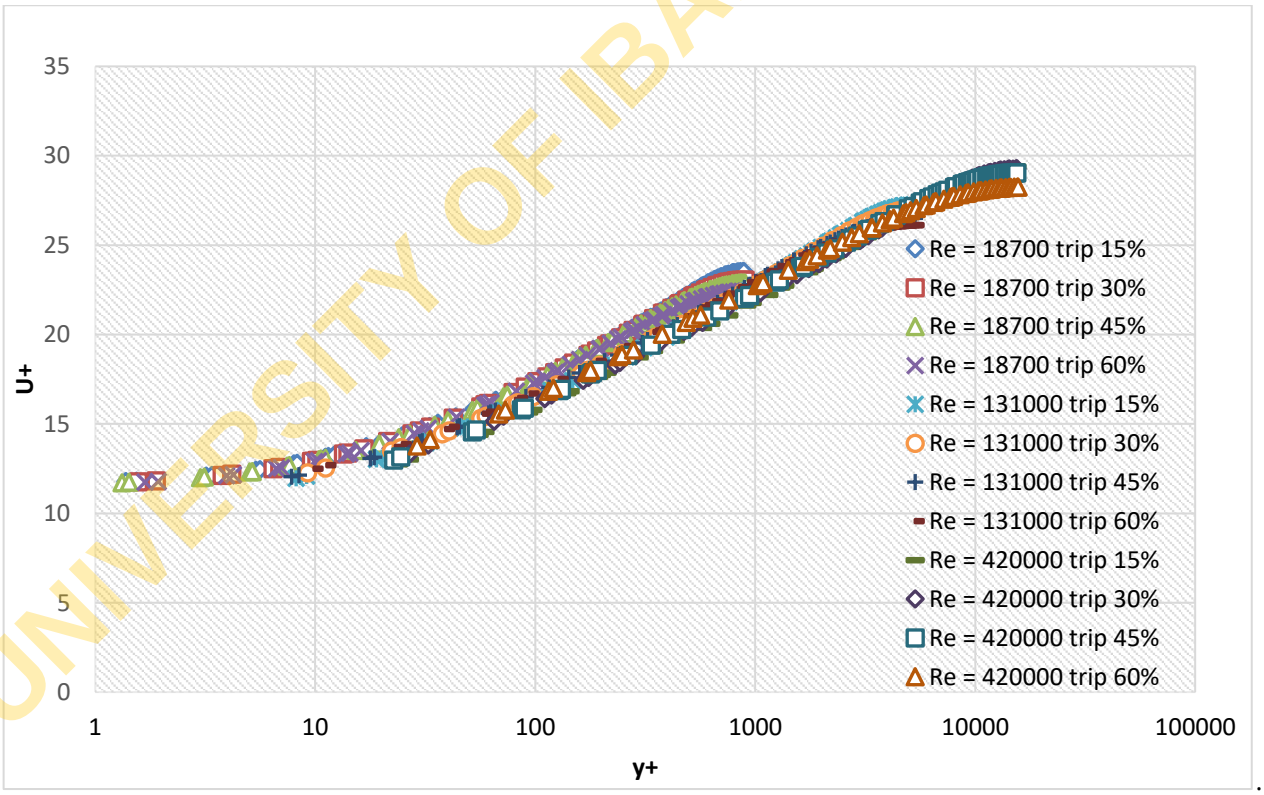

Figure-9. Normalized velocity distribution for flow with tripping.

4. CONCLUSIONS

Numerical analysis has been performed using the standard k-ϵ turbulence model to study the effects of entry conditions on the characteristics of channel flow. The flow is simulated for various degrees of tripping under the same conditions. The trends observed are in agreement with existing literature. It was discovered that tripping devices placed at the entry of an open channel to cause immediate transition from laminar to turbulent boundary layer, cause an increase in the value of the skin friction coefficient by a factor between 2 and 11%. Thus the tripping devices could be likened to roughness elements placed in the bed of a

channel which experimental works have reported to increase the value of the skin friction coefficient.

Declaration of Conflict of Interest

The authors declare that there is no conflict of interest regarding the publication of this article. All authors read and contributes to this article.

REFERENCES

Afzal B., Al Faruque M. and Balachandar R. 2009. Effects of Reynolds Number, Near-Wall Perturbation and Turbulence on Smooth Open-Channel Flows. Journal of Hydraulic Research. 47(1): 66-81.

Al Faruque M.D., Wolcott S., Goldowitz J. and Wolcott T. 2014. Open Channel Flow Velocity Profiles for Different Reynolds Numbers and Roughness Conditions. International Journal of Research in Engineering and Technology. 3(1): 400-405.

Al-Salaymeh A. and Bayoumi O.A. 2009. Investigations of Tripping Effect on the Friction Factor in Turbulent Pipe Flows. Journal of Fluids Engineering. 131, 3-10.

Bonakdari, H., Lipeme-Kouyi, G. and Asawa, L.G. 2014. Developing Turbulent Flows in Rectangular Channels: A parametric study. Journal of Applied Research in Water and Wastewater. 1(2): 53-58.

Cardoso A.H., Graf W.H. and Gust G. 1989. Uniform flow in a Smooth Open Channel. Journal of Hydraulic Research. 27(5): 603-616.

Ferziger J. H. and Peric M. 2002. Computational methods for fluids dynamics. (3rd ed.). Berlin: Springer.

Kirkgoz S.M. 1989. Turbulent Velocity Profiles For Smooth and Rough Open Channel Flow. Journal of Hydraulic Engineering. 115(11): 1543-1561.

Kirkoz S.M. and Ardichoglu M. 1997.Velocity Profiles of Developing and Developed Open Channel Flow. Journal of Hydraulic Engineering. 123(12): 1099-1105.

Nezu I. 2005. Open-Channel Flow Turbulence and Its Research Prospect in the 21st Century. Journal of Hydraulics Engineering. 131(4): 229-246.

Ranga Raju K.G., Asawa G.L. and Mishra H.K. 2000. Flow-Establishment Length in Rectangular Channels and Ducts. Journal of Hydraulic Engineering. 126(7): 533-539.

Tominaga A. and Nezu I. 1992. Velocity Profiles in Steep Open-Channel Flows. Journal of Hydraulic Engineering. 118(1): 73-90.

Tominaga A., Nezu I., Ezaki K. and Nakagawa H. 1989. Three-dimensional Turbulent Structure in Straight Open Channel Flows. Journal of Hydraulic Research. 27(1): 149-173.

Wilcox D. C. 2006. Turbulence modeling for CFD (3rd ed.). California: DCW.

Yan J., Tang H., Xiao Y., Li K. and Tian Z. 2011. Experimental Study on Influence of Boundary on Location of Maximum Velocity in Open Channel Flows. Water Science and Engineering. 4(2): 185-191.

Yang S., Tan S. and Lim S. 2004. Velocity Distribution and Dip-Phenomenon in Smooth Uniform Open Channel Flows. Journal of Hydraulic Engineering. 130(12): 1179-1186.

NOMENCLATURE

h	channel height
F	Froude number
Re	Reynolds number
U^*	Friction velocity
U	mean flow velocity
U_e	free-stream velocity
Le	Length of flow developing zone
ν	kinematic viscosity
ν_T	turbulent kinematic viscosity
g	acceleration due to gravity
ρ	density
C_f	skin friction coefficient
K	von-karman constant
B	width of channel
U^+	normalized velocity
$y+$	normalized vertical height
k	turbulent kinetic energy
ϵ	rate of dissipation